The Astrophysical Journal, 993:202 (8pp), 2025 November 10 https://doi.org/10.3847/1538-4357/ae11a7

Using LHASSO-observed Gamma-Ray Bursts to Study the Extragalactic Background Light

Longhua Qin[1], Jiancheng Wang[2,3], Chuyuan Yang[2,3], Quangui Gao[1], Huaizhen Li[1], Ju Ma[1], Weiwei Na[1], Ao Wang[1], Xu Zhang[1], Baoyu Ma[1], Tingfeng Yi[4], Zunli Yuan[5], and Chunxia Gu[6]
[1] Department of Physics, Yuxi Normal University, Yuxi, Yunnan, 653100, People's Republic of China; qggao@yxnu.edu.cn, lhz@yxnu.edu.cn, mj@yxnu.edu.cn
[2] Yunnan Observatory, Chinese Academy of Sciences, Kunming, Yunnan, 650011, People's Republic of China; chyy@ynao.ac.cn
[3] Key Laboratory for the Structure and Evolution of Celestial Objects, Chinese Academy of Sciences, Kunming, Yunnan, 650011, People's Republic of China
[4] Department of Physics, Yunan Normal University, Kunming, Yunnan, 650092, People's Republic of China
[5] Department of Physics and Synergistic Innovation Center for Quantum Effects and Applications, Hunan Normal University, Changsha, Hunan, 410081, People's Republic of China
[6] Oxbridge College, Kunming University of Science and Technology, Kunming, Yunnan, 650011, People's Republic of China
Received 2025 April 6; revised 2025 September 15; accepted 2025 October 8; published 2025 November 5

Abstract

The extragalactic background light (EBL), a diffuse radiation field produced by all galaxies throughout cosmic history, plays a crucial role in the propagation of high-energy gamma-rays through photon–photon interactions. These interactions lead to characteristic absorption features in the observed TeV gamma-ray spectrum. Motivated by these effects, we analyze observations of GRB 221009A, the most energetic gamma-ray burst (GRB) ever detected by the Large High Altitude Air Shower Observatory, to investigate the EBL via gamma–gamma absorption signatures imprinted on the TeV spectrum. To minimize potential effects from Lorentz invariance violation and axion-like particles, we restrict our analysis to gamma rays with energies below 8 TeV. By comparing the modeled intrinsic spectra with the observed data, we constrain the spectral energy distribution of the EBL in the wavelength range of 0.1–40 μm. Our results are consistent with existing EBL models and observational limits derived from galaxy counts and infrared surveys. Furthermore, the inferred cosmic emissivity, which represents the integrated light from galaxies, is found to be primarily dominated by spiral-type galaxies.

Unified Astronomy Thesaurus concepts: Gamma-ray bursts (629); Cosmic background radiation (317)

1. Introduction

The extragalactic background light (EBL) refers to the diffuse radiation field that permeates the Universe, originating from the integrated light emitted by all galaxies and other astrophysical sources throughout cosmic history. Accurate measurement and comprehensive understanding of the EBL are crucial for a wide range of studies in astrophysics and cosmology. The EBL encodes valuable information about the history of galaxy and large-scale structure formation, the evolution of stellar populations, and the processes governing the production and distribution of heavy elements. Moreover, it is directly linked to the cosmic star formation rate density and the initial mass function (Y. Inoue et al. 2013; A. Saldana-Lopez et al. 2021). Additionally, the EBL plays a critical role in the propagation and interaction of high-energy cosmic rays and gamma rays, rendering its characterization essential for the accurate interpretation of observations from gamma-ray telescopes. For a detailed elaboration, see E. Dwek & F. Krennrich (2013).

Direct measurements of the EBL face several significant challenges. Chief among them is the difficulty of removing contamination from foreground emissions, such as zodiacal light originating from interplanetary dust within the solar system and stellar light from the Milky Way (M. G. Hauser et al. 1998; M. G. Hauser & E. Dwek 2001; K. Mattila 2006). Previous efforts to measure the EBL have primarily concentrated on the optical (R. A. Bernstein 2007; T. R. Lauer et al. 2021) and infrared (IR; R. A. Bernstein 2007) regimes. However, no consensus has been reached regarding the reliability of these datasets, and calibration issues remain widespread in practical observations. A robust lower limit on the EBL intensity can be established by summing the light from individually resolved galaxies (P. Madau & L. Pozzetti 2000; M. G. Hauser & E. Dwek 2001). This method is applicable across multiple wavelengths—including ultraviolet (UV), optical/near-infrared (NIR), far-infrared, and submillimeter—and is particularly valuable for constraining the local EBL. Typically, the EBL intensities derived via this galaxy-count method in the optical and NIR bands are lower than those inferred from direct photometric measurements.

A powerful method for studying EBL is leveraging the interaction between high-energy gamma-ray photons traveling across cosmological distances and the EBL through pair production ($\gamma\gamma \rightarrow e^+e^-$). This interaction imprints an absorption feature in the observed spectra of these gamma rays. By carefully analyzing these features, we can infer the spectral energy distribution (SED) of the EBL and place constraints on its evolution with redshift (F. W. Stecker & O. C. de Jager 1993; E. Dwek & J. Slavin 1994; M. Meyer et al. 2012; A. Domínguez et al. 2013; A. Desai et al. 2017, 2019; H. E. S. S. Collaboration et al. 2017; Fermi-LAT Collaboration et al. 2018; L. Qin et al. 2023; L. J. Dong et al. 2023). Gamma-ray bursts (GRBs) stand out as some of the most energetic phenomena in the Universe. The Large High Altitude Air Shower Observatory (LHAASO), boasting

unprecedented sensitivity in the TeV energy range and a wide field of view, has created a new avenue for the systematic study of GRBs and their connection to the EBL (Z. Cao et al. 2019). Among the GRBs observed by LHAASO, GRB 221009A is particularly remarkable (Z. Cao et al. 2019, 2023; H. Abdalla et al. 2024) and the most energetic GRB ever recorded, with a redshift of 0.151 (A. de Ugarte Postigo et al. 2022). Its broad energy coverage and substantial photon flux offer a unique opportunity to explore the EBL-induced attenuation over cosmological distances. Overall, the data from GRB 221009A detected by LHAASO can significantly advance our understanding of the EBL's properties and its role in the Universe.

GRB 221009A is employed to study the EBL. The research mainly focuses on the investigation of the reduced EBL absorption of high-energy TeV photons during their cosmological propagation due to Lorentz invariance violation (LIV) (see e.g., J. D. Finke & S. Razzaque 2023) and axion-like particles (ALPs) (see e.g., D. Avila Rojas et al. 2024). Some papers have presented the SED of the EBL constrained by the observations from LHAASO. However, the EBL SED obtained in these studies may not have excluded the effects of LIV and ALPs (Z. Cao et al. 2023). Moreover, the process of reconstructing the EBL spectrum is not well defined. Therefore, considering the influence of LIV and ALPs on photons with energies greater than 8 TeV, we attempt to truncate the energy spectrum observed by LHAASO at 8 TeV. Considering that gamma rays with energy $E_{\rm gamma}$ are absorbed via $\gamma\gamma$ pair production interactions with soft photons of wavelength $\lambda_{\rm EBL} \sim [0.5\ \mu{\rm m} - 5\ \mu{\rm m}] \times \left(\frac{E_\gamma}{1\,{\rm TeV}}\right) \times (1+z)^2$, LHASSO observations of TeV gamma rays can therefore be used to constrain the SED of the EBL at wavelengths shorter than $\sim$40 μm (A. Albert et al. 2022).

We employ five theoretical EBL models, namely, those proposed by A. Domínguez et al. (2011), R. C. Gilmore et al. (2012), A. Franceschini & G. Rodighiero (2017), A. Saldana-Lopez et al. (2021), and J. D. Finke et al. (2022). The EBL optical depth is computed using the publicly available code ebltable,[7] which allows us to interpret the observed attenuation patterns. We adopt a Bayesian approach to select the optimal intrinsic spectral model from five candidates: power law, log-parabola, power law with exponential cutoff, log-parabola with exponential cutoff, and broken power law (see e.g., A. Donath et al. 2023). These spectral models are evaluated under the attenuation relation

$$F_{\rm obs}(E_\gamma) = F_{\rm int}(E_\gamma) e^{-k\tau(E_\gamma, z)}, \tag{1}$$

where $F_{\rm obs}(E_\gamma)$ and $F_{\rm int}(E_\gamma)$ are the observed and intrinsic fluxes, respectively, $\tau(E_\gamma, z)$ is the EBL optical depth, and k is a scaling factor.

To select the intrinsic spectral model, we fix $k = 1$ and adopt a representative EBL optical depth template—specifically, the Saldana–Lopez model (A. Saldana-Lopez et al. 2021). This ensures that the intrinsic spectral shape is determined independently of any scaling in EBL attenuation. We then evaluate the goodness of fit for each candidate model and identify the one with the lowest Akaike information criterion (AIC) as the best representation of the intrinsic spectrum.

Using this selected intrinsic model, we proceed to fit the observed spectra with each of the five classical EBL models, now allowing the scaling factor k to vary as a global parameter across all energy bins (see, e.g., Fermi-LAT Collaboration et al. 2018; A. Desai et al. 2019). This yields five best-fit values k_i, each corresponding to a different EBL template. These fits provide constraints on the EBL intensity and spectral shape in a model-dependent but internally consistent manner.

Unlike the method of L. Gréaux et al. (2024), which allows k to vary with energy, we adopt a single global scaling parameter to reduce the number of free parameters—a necessary simplification given the limited observational data. To improve the robustness of our results, we include multiple EBL optical depth templates in the analysis. Finally, instead of performing stacking (Fermi-LAT Collaboration et al. 2018; A. Desai et al. 2019), which also requires large datasets to be effective, as noted by, e.g., L. Qin et al. (2023), we adopt a simple averaging strategy across sources to reduce statistical fluctuations. We also explore the implications for cosmic emissivity, offering insights into the integrated light from galaxies over cosmic time.

In this work, a flat ΛCDM cosmology is adopted, where $\Omega_\Lambda = 0.7$, $\Omega_M = 0.3$, and $H_0 = 70\,{\rm km\,s^{-1}\,Mpc^{-1}}$. Additionally, the unprimed and primed quantities denote the quantities in the observer's frame and the comoving frame, respectively.

2. Model and Strategy

We used the Bayesian inference Python package UltraNest (J. Buchner 2021) to derive posterior probability distributions for the best-fit SED model parameters. We also computed the Bayesian evidence, a key metric for model comparison. For model selection, we chose the SED model with the lowest AIC value. The AIC is given by AIC$=2k_n - 2{\rm Ln}(\hat{L})$, where k_n is the number of estimated parameters and $\hat{L}$ is the maximized likelihood. This approach provides an objective and quantitative way to assess models, selecting the one that balances goodness of fit and model complexity.

In the abovementioned way, we obtain the optimal intrinsic spectrum of the GRB. Then, we use five different EBL optical depth models for fitting and obtain five different scale parameters k. We derive the final optical depth and uncertainty by calculating the mean of four scaled individual optical depths.

We obtained the optical depth data of $\overline{\tau}(E_\gamma, z)$ and σ_τ and then reconstructed the SED of the EBL. For a given volume emissivity $j(\lambda, z')$ that evolves with redshift, the SED of the EBL can be derived by (see, e.g., A. Saldana-Lopez et al. 2021)

$$\lambda I_\lambda(\lambda, z_i) = \frac{c^2}{4\pi\lambda} \int_{z_i}^{z_{\rm max}} j(\lambda(1+z_i)/(1+z'), z') \left|\frac{dt}{dz'}\right| dz', \tag{2}$$

where

$$\frac{dt}{dz'} = \frac{-1}{H_0(1+z')\sqrt{\Omega_m(1+z')^3 + \Omega_\Lambda}}, \tag{3}$$

and the volume emissivity $j(\lambda_i, z)$ evolves with redshift based on a function similar to the star-formation history (SFH) parameterization of P. Madau & M. Dickinson (2014), leading

[7] https://github.com/me-manu/ebltable/

to the expression

$$j(\lambda, z) = j_0(\lambda) \cdot \frac{(1+z)^{b_i}}{1 + \left(\frac{1+z}{c_i}\right)^{d_i}}, \quad (4)$$

where we adopt the methodology from Fermi-LAT Collaboration et al. (2018), modeling the cosmic emissivity as a sum of normal templates with fixed peak positions:

$$j_0(\lambda) = \sum_i a_i \cdot \exp\left[-\frac{(\log\lambda - \log\lambda_i)^2}{2\sigma^2}\right] \quad [\mathrm{erg \cdot s^{-1} \cdot cm^{-3} \cdot Hz^{-1}}]. \quad (5)$$

Here we set $\sigma = 0.5$ and $\lambda_i = [0.17, 0.92, 2.2, 8.0, 16, 50]$. We used the values provided by Fermi-LAT Collaboration et al. (2018) for our first four peak positions and employed the values of 16 and 50 μm from A. Desai et al. (2019) as supplements to the spectral shape in the mid-infrared band. In fact, we also attempted some fine-tuning and found that the above combination could provide a better fit to the cosmic emissivity.

The EBL-induced attenuation of the gamma-ray flux at energy E_γ, observed at redshift z, is described by the optical depth, integrated over redshift $z' \leqslant z$, and ϵ' and $\mu' = 1 - \cos\theta'$ are comoving EBL photon energy and the cosine of the angle for the incident photons, respectively:

$$\tau(E_\gamma, z) = \int_0^z dz' \frac{\partial L}{\partial z'}(z') \int_0^\infty d\epsilon' \frac{4\pi}{c} \frac{\nu I_\nu(\epsilon', z')}{\epsilon'^2} \int_{-1}^1 d\mu' \frac{1-\mu'}{2} \sigma_{\gamma\gamma}(E_\gamma(1+z'), \epsilon', \mu'). \quad (6)$$

Here, νI_ν is the EBL specific intensity measured in units nW m^{-2} sr^{-1} and $\sigma_{\gamma\gamma}$ is the Breit–Wheeler cross section (see e.g., J. Biteau & D. A. Williams 2015). For a flat ΛCDM cosmology, the distance element is given by $\frac{\partial L}{\partial z} = \frac{c}{H_0}(1+z)^{-1}(\Omega_\Lambda + \Omega_m(1+z)^3)^{-1/2}$.

Given the above constraints, we use the Markov Chain Monte Carlo (MCMC) method to explore the multidimensional parameter space and estimate model parameter uncertainties based on observed data. This Bayesian approach considers a set of parameters (hereafter $\boldsymbol{\theta}$) given the data, with the likelihood function defined as

$$-\ln L(\text{ data }|\boldsymbol{\theta}) \propto \sum_{i=1}^N \left(\frac{\tau_{\rm data}(E_i, z) - \tau_{\rm model}(\boldsymbol{\theta}|E_i, z)}{\sigma_i}\right)^2, \quad (7)$$

where $\tau_{\rm model}(\boldsymbol{\theta}|E_i, z)$ is the model optical depth obtained by Equation (6), N is the number of data points, and $\tau_{\rm data}(E_i, z)$ and σ_i are the optical depth and its uncertainty obtained from the SED fitting result, respectively.

We perform the MCMC analysis using the publicly available code CosmoMC,[8] developed by A. Lewis & S. Bridle (2002) and D. J. C. Mackay (2003). The algorithm requires an input likelihood function of Equation (7), initial parameter values, and the number of Monte Carlo samples. By iterating through the parameter space, the probability density functions of model parameters are asymptotically approached as the sample size increases.

[8] http://cosmologist.info/cosmomc/

Table 1
The AIC Values for Five Different Intrinsic Spectra

Name	PL	BPL	ECPL	LP	LPC
WD 231-240 s	**4.21**	8.07	6.87	6.21	8.95
WD 240-248 s	**5.14**	8.82	8.14	7.16	10.28
WD 248-326 s	**6.80**	8.95	7.57	7.58	9.58
WD 326-900 s	7.12	8.56	**6.28**	6.57	8.30
WD+KM230-300 s	**10.28**	10.79	17.21	12.30	19.35
WD+KM300-900 s	9.13	9.23	7.20	**7.14**	9.19

Note. The best models with the lowest AIC values are shown in boldface. The five different intrinsic spectra are as follows: the power Law (PL), the broken power law (BPL), the power law with exponential cutoff (ECPL), the log-parabola (LP), and the log-parabola with exponential cutoff (LPC).

3. Application and Results

Here, we present the Water Cherenkov Detector Array (WCDA) and Kilometer Squared Array (KM2A) observations from LHAASO within four distinct time intervals. Due to pileup effects, the WCDA data in the intervals 231–240 and 248–326 s are treated as lower limits. For the 326–650 s interval, a narrow time bin centered around 510 s is excluded for the same reason. More detailed information can be found in LHAASO Collaboration et al. (2023). In addition, we include WCDA and KM2A data covering two broader time intervals: 230–300 and 300–900 s, as reported in Z. Cao et al. (2023).

Based on these observations, we categorize the data as follows: four WCDA-only datasets—WD 231-240, WD 240-248, WD 248-326, and WD 326-900 s. Two additional combinations involve both WCDA and KM2A data: WD+KM230-300 and WD+KM300-900 s. For further details, please refer to Z. Cao et al. (2023). Due to the truncation of 8 TeV data and the limited availability of KM2A measurements, we do not include combinations involving KM2A alone.

Following the methodology described above, we analyzed six groups of observational data. For each group, we considered five candidate intrinsic spectral shapes and evaluated their performance using the AIC method, assuming an optical depth model from A. Saldana-Lopez et al. (2021) with a fixed scaling factor $k = 1$. The best-fitting intrinsic spectral models for each data group are summarized in Table 1. To ensure robustness, we repeated the same model selection procedure using four additional EBL optical depth templates. The results remained consistent across all cases, confirming the stability of our model selection. Notably, the log-parabola with an exponential cutoff was not favored as the intrinsic spectral shape for any of the GRBs analyzed.

Starting from the best intrinsic spectra above, we fitted five widely used EBL templates (A. Domínguez et al. 2011; R. C. Gilmore et al. 2012; A. Franceschini & G. Rodighiero 2017; A. Saldana-Lopez et al. 2021; J. D. Finke et al. 2022) to obtain the scale factors k_i and their uncertainties $\sigma_{k,i}$ for each dataset (see Table 2). For each template i and photon energy E, we compute the template-adjusted optical depth $\tau_{i,\rm der}(E)$ and its propagated uncertainty as

$$\tau_{i,\rm der}(E) = k_i\, \tau_{i,\rm model}(E), \qquad \sigma_{\tau,i}(E) = \tau_{i,\rm model}(E)\, \sigma_{k,i}, \quad (8)$$

where $\tau_{i,\rm model}(E)$ is the optical depth predicted by template i. The final optical depth at each energy is then taken as the

Table 2
The Parameter Values of the Scale Parameters k Obtained through Fitting SEDs of GRB 221009A under Five EBL Optical Depth Temples

Name	Dominguez	Finke2022	Franceschini2017	Gilmore	Saldana–Lopez
WD 231-240 s	1.7 ± 0.57	1.9 ± 0.71	1.6 ± 0.58	1.8 ± 0.61	1.7 ± 0.63
WD 326-900 s	2.2 ± 0.37	1.6 ± 0.39	1.3 ± 0.35	2.4 ± 0.44	1.8 ± 0.41
WD 240-248 s	1.7 ± 0.55	1.7 ± 0.66	1.5 ± 0.56	1.8 ± 0.60	1.7 ± 0.61
WD 248-326 s	2.1 ± 0.45	1.5 ± 0.41	1.3 ± 0.37	2.4 ± 0.51	1.7 ± 0.44
WD+KM230-300 s	1.4 ± 0.28	1.0 ± 0.10	0.80 ± 0.081	1.7 ± 0.39	1.0 ± 0.12
WD+KM300-900 s	1.5 ± 0.51	0.94 ± 0.29	0.69 ± 0.22	1.7 ± 0.59	1.0 ± 0.30

arithmetic mean across the five templates:

$$\tau_{\rm final}(E) = \frac{1}{N}\sum_{i=1}^{N} \tau_{i,\rm der}(E) \quad (N = 5). \tag{9}$$

To reflect both the statistical uncertainty from the k-fits and the systematic spread among templates, we compute the final uncertainty as the quadrature sum of the mean propagated uncertainty and the inter-model variance:

$$\sigma_{\rm final}(E) = \sqrt{\frac{1}{N}\sum_{i=1}^{N} \sigma_{\tau,i}^2(E) \; + \; {\rm Var}_i[\tau_{i,\rm der}(E)]}\,. \tag{10}$$

Here the first term represents the average propagated uncertainty due to the fitted k_i, and the second term captures the systematic dispersion arising from different EBL templates. The SED fits obtained with the Saldana–Lopez template are shown in Figure 1 (best fits and 99.7% intervals); the resulting $\tau_{\rm final}(E)$ and $\sigma_{\rm final}(E)$ are plotted and compared with the Saldana–Lopez model in Figure 2.

As shown in Table 2, the best-fit values of the scaling factor k obtained from individual datasets exhibit a dispersion of approximately 30%–50%. This level of scatter propagates into the reconstructed EBL optical depths and is further amplified in the cosmic emissivity calculation (by a multiplicative factor on the order of 10^{25}). As a result, the formal confidence intervals become excessively broad and of limited interpretive value. To avoid this, we do not present error bands dominated by such amplified uncertainties. Instead, we classify the datasets into two observational configurations: (1) WCDA-only and (2) WCDA+KM2A combined. For each configuration, the corresponding subgroups (four for WCDA-only and two for WCDA+KM2A) were analyzed separately to reconstruct the EBL spectrum and cosmic emissivity based on their best-fit k values. We then adopt the median of the four WCDA-only reconstructions and the median of the two WCDA+KM2A reconstructions as the final representative results for each case. This approach emphasizes the central tendency of the derived constraints while mitigating the misleading effects of overly broad error bands.

For consistency with previous studies, all reconstructed quantities are converted to their local values at $z = 0$. The fitting parameters a_i, b_i, c_i, and d_i, derived from Equations (4) and (5), describe the redshift evolution of the comoving volume emissivity. Substituting these into Equation (2) and setting $z_i = 0$, we obtain the EBL spectrum at the present epoch. The consolidated results are presented in Figure 3, providing a comparative overview of the EBL spectrum and cosmic emissivity under different observational setups.

4. Discussion and Conclusions

In this study, we conducted a systematic investigation of the EBL by analyzing TeV gamma-ray observations from GRB 221009A. Using data from the WCDA and KM2A detectors of LHAASO, we reconstructed the EBL SED and examined the corresponding cosmic emissivity at redshift $z = 0$.

While our results, as shown in Figure 3, do not exhibit significant deviations from established EBL models, this work represents the first systematic constraint on the EBL spectrum below 40 μm using LHAASO observations. Our results lie slightly above those derived from galaxy-counting methods such as GAMA–DEVILS–Hubble Space Telescope (HST); (S. Koushan et al. 2021) and JWST/NIRCam (R. A. Windhorst et al. 2023), as compiled in J. Biteau (2023), which are commonly considered to provide the lower bound of the EBL. Similarly, our results are marginally higher than those predicted by the Saldana–Lopez model, which is based on direct observations of galaxies across UV to far-infrared wavelengths. As such, it may underestimate contributions from faint or unresolved sources, a limitation shared with traditional galaxy-counting approaches. Nevertheless, in the 1–5 μm wavelength ranges, the results from GAMA–DEVILS–HST, JWST/NIRCam, and the Saldana–Lopez model show strong mutual consistency.

To ensure robustness, we carefully considered a broad range of intrinsic spectral shapes and applied the reconstruction method proposed by Fermi-LAT Collaboration et al. (2018) to derive the EBL energy density and its associated cosmic emissivity in a self-consistent manner. Taken together, these efforts provide a coherent and reproducible framework for constraining the EBL based on TeV gamma-ray observations. Furthermore, our derived cosmic emissivity values are generally consistent with those reported by A. Domínguez et al. (2011) and A. Saldana-Lopez et al. (2021), supporting the interpretation that the EBL is primarily shaped by the SED of spiral-type galaxies.

LHASSO observed approximately 18 TeV gamma photons from GRB 221009A, and HAWC's Charpet 2 detected 251 TeV gamma photons. These results, which would have been impossible to be detected previously, may confirm the existence of ALPs (see e.g., D. Avila Rojas et al. 2024) or the effects of LIV (see, e.g., J. D. Finke & S. Razzaque 2023). It is even possible that both factors act together, leading to a reduction in the absorption effect of the EBL on gamma photons. First, if ALPs exist, part of the electromagnetic flux from TeV radiation sources may be converted into axion-like particles in the magnetic field of the host galaxy and the intergalactic magnetic field along the photon propagation path (see e.g., D. Avila Rojas et al. 2024). These axion-like particles will propagate toward Earth and may reconvert into photons in the Galactic magnetic field. Therefore, axion-like

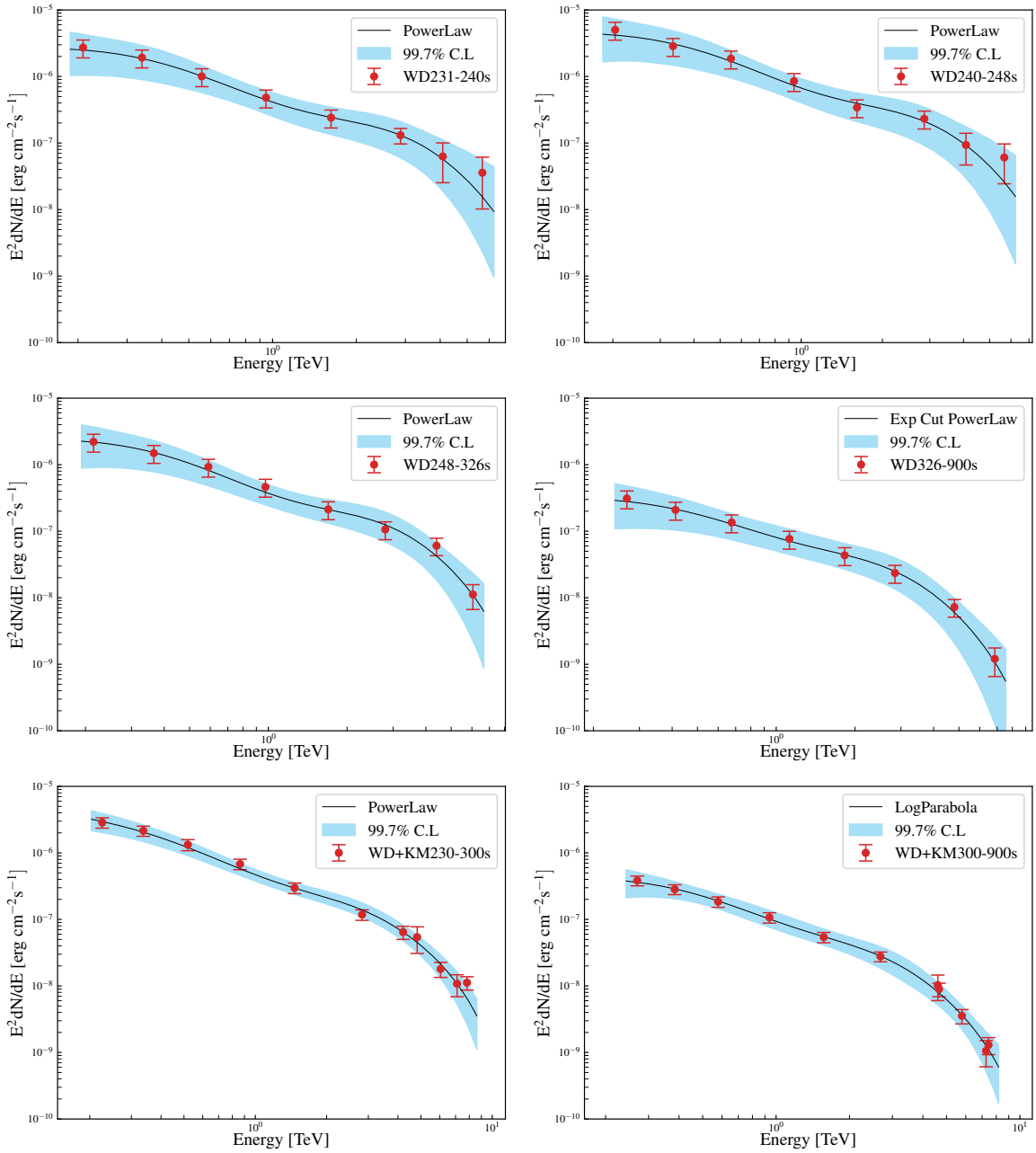

Figure 1. The best-fitting SEDs of the GRB 221009A under the EBL model of A. Saldana-Lopez et al. (2021).

particles provide a new way for high-energy photons to travel long distances, bypassing the traditional absorption by EBL. To understand this process in depth, a more detailed understanding of the interstellar and Galactic magnetic fields is required. Additionally, LIV effects can cause astrophysical changes, one of which is the energy-dependent speed of photons, resulting in a slight time difference between gamma photons at different wavelengths during propagation (see, e.g., D. Avila Rojas et al. 2024). Furthermore, LIV effects also raise the threshold for photon absorption, weakening the absorption of gamma photons by EBL. To assess this effect, a deep understanding of the quantum gravity energy scale is needed, which imposes stricter requirements on the observational capabilities of gamma-ray telescopes. Therefore, due to these factors, constraining the EBL energy distribution using TeV gamma photons becomes more difficult if $\lambda_{\rm EBL} > 40\,\mu$m (comparing with $E_\gamma > 8$ TeV). As a result, in this work, we only focus on constraining certain components of the EBL leveraging very high-energy radiation sources.

Our results are compared with existing EBL models and observations, such as those presented in A. Saldana-Lopez et al. (2021) and C. Papovich et al. (2004), as shown in Figure 3. The EBL densities derived using WCDA-only data and the WCDA+KM2A combination are slightly higher than the other results. Nevertheless, all values generally lie within the range bounded by galaxy counts (P. Madau & L. Pozzetti 2000) and direct infrared measurements (see, e.g., D. Elbaz et al. 1999; R. A. Bernstein et al. 2002; G. G. Fazio et al. 2004; C. Papovich et al. 2004; E. L. Wright 2004; T. Matsumoto et al. 2005; R. S. Savage & S. Oliver 2005). Moreover, our results show no significant indication that the Universe is more transparent to high-energy gamma rays than predicted, in

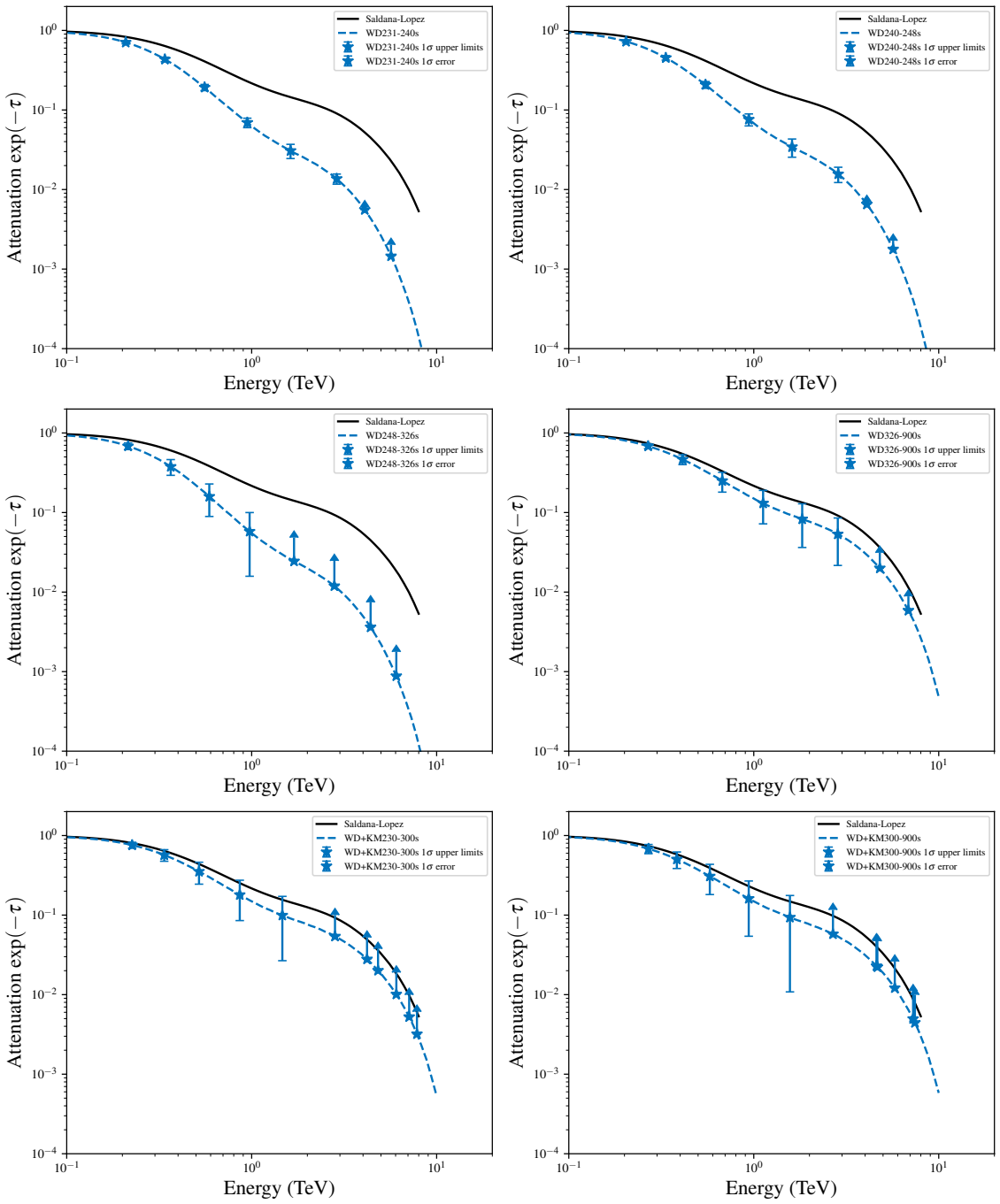

Figure 2. Comparison of the optical depth derived from spectral fitting with the EBL model by A. Saldana-Lopez et al. (2021).

agreement with the conclusions of A. Franceschini et al. (2019).

Regarding the cosmic emissivity, except for the WCDA +KM2A case, we find that the derived NIR values are broadly consistent with those reported in A. Domínguez et al. (2011) and A. Saldana-Lopez et al. (2021), while the mid-infrared values appear somewhat lower. A likely reason is that the assumed Gaussian form of the emissivity spectrum (see Equation(4)) is not well constrained in this wavelength range due to limited observational data.

It is also worth emphasizing that, due to the substantial dispersion in the scaling factor k across datasets, we did not derive traditional confidence intervals for the EBL energy density and cosmic emissivity. Instead, for each observational group, we used the median of the best-fit results as the final estimate. This approach effectively reduces the impact of large uncertainties in k and the resulting propagation into the optical depth and emissivity, providing more stable and representative outcomes under current data limitations.

Finally, we emphasize the importance of distinguishing between the WCDA and KM2A datasets as they cover different and complementary energy regimes (see e.g., Z. Cao et al. 2023). Properly accounting for the energy-dependent coverage helps us to improve constraints on the intrinsic spectrum of the sources. Maximizing the use of all available spectral information is essential for obtaining robust and accurate estimates of the EBL.

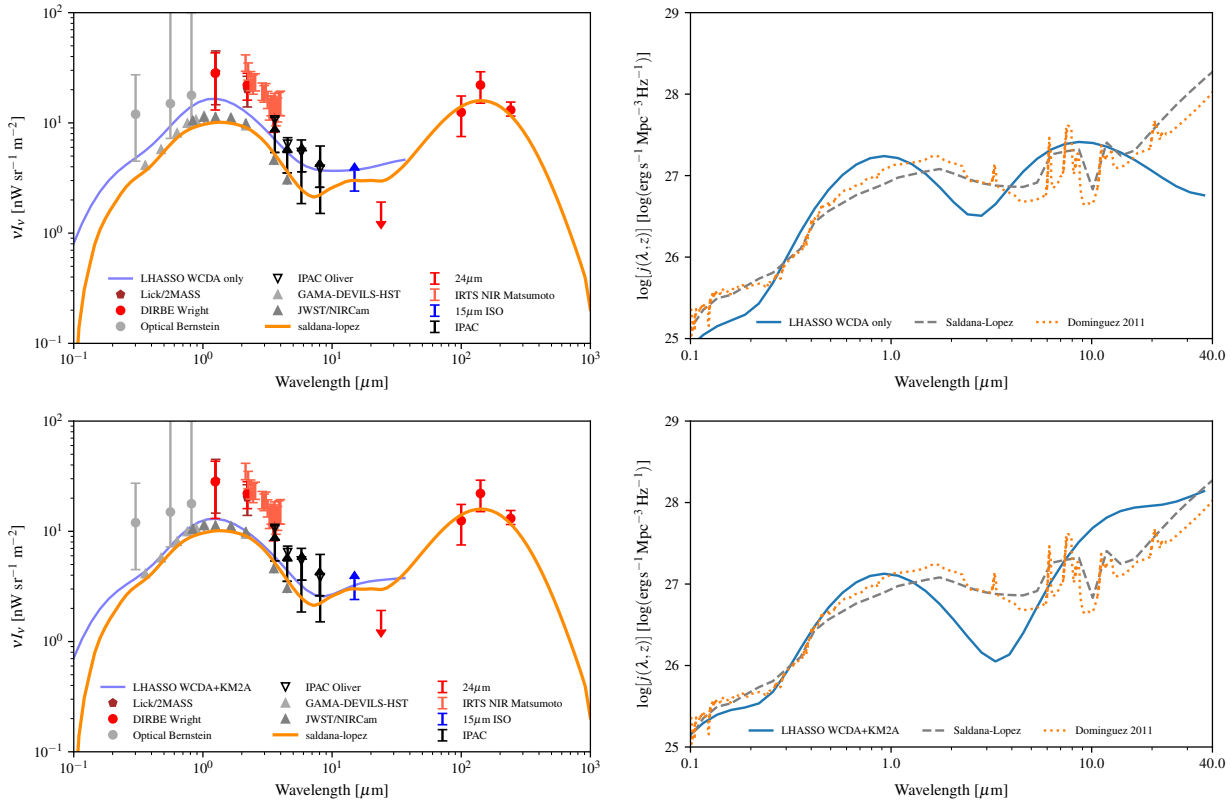

Figure 3. Left panel: constraints on the EBL as a function of wavelength at $z = 0$, ranging from 0.1 to 40 μm, compared with various surveys—24 μm and MIPS data from C. Papovich et al. (2004), Lick/Two Micron All Sky Survey from E. L. Wright (2001), DIRBE Wright from E. L. Wright (2004), optical data from Bernstein (R. A. Bernstein et al. 2002), IRTS NIR Matsumoto (T. Matsumoto et al. 2005), 15 μm ISO from D. Elbaz et al. (1999), GAMA–DEVILS–HST from S. Koushan et al. (2021), JWST/NIRCam for R. A. Windhorst et al. (2023), and IPAC data from G. G. Fazio et al. (2004) and R. S. Savage & S. Oliver (2005). Right panel: the derived cosmic emissivity (luminosity density), comparing with data from A. Domínguez et al. (2011) for Dominguez 2011 and A. Saldana-Lopez et al. (2021) for Saldana–Lopez. Final results are taken as the medians of four WCDA-only and two WCDA+KM2A reconstructions.

This study presents a comprehensive analysis of the EBL spectrum using TeV gamma-ray observations. Despite existing uncertainties, our results are roughly consistent with established models and offer new insights into the the cosmic emissivity. Compared with more recent study carried by L. Gréaux et al. (2024), our results are generally consistent within the wavelength range of 0.6–7.0 μm. However, in the region below 0.6 μm, the EBL spectral intensity we derived is lower. This discrepancy may be attributed to the limited observational data available from LHAASO, suggesting that additional data are required to improve the constraints. Furthermore, our results indicate that beyond 40 μm, the EBL spectral values tend to be lower than those predicted by classical EBL models, such as the A. Saldana-Lopez et al. (2021), and a similar trend is also seen in L. Gréaux et al. (2024). A plausible explanation is that, at wavelengths longer than 40 μm, the corresponding TeV photons experience reduced EBL absorption due to possible effects from ALPs and LIV, leading to an underestimation of the EBL intensity in this regime. In addition, further observational and theoretical efforts are essential to refine these constraints and enhance our understanding of the Universe's photon environment. In terms of the results of constraining the EBL using TeV gamma rays, there may also be some problems in this paper. For example, there may be issues with the assumed intrinsic spectral functions because they may not be able to cover the true spectral shapes. Moreover, introducing a single overall scale factor k for each set of the EBL optical depth also has its drawbacks since it is problematic to have the same amplification coefficient for each energy band. Therefore, in the future, when using the intrinsic spectra, assumptions based on radiation mechanisms can be adopted, but this requires a sufficient number of (quasi-) simultaneous multi–wave band SEDs. Alternatively, statistical methods can be used to obtain the intrinsic spectra, such as the copula method. Copulas are functions that link a multivariate distribution to its one-dimensional marginal distributions (R. B. Nelson 2006). According to Sklar's theorem, if $H(x, y)$ is a joint distribution with continuous marginals $F(x)$ and $G(y)$, then there exists a unique copula C such that $H(x, y) = C(F(x), G(y))$. This allows the dependence structure between variables to be modeled separately from their marginal distributions, with all correlation information encapsulated by the copula. This method has been applied to the study of statistical correlations between the X band and the UV band (see e.g., Z. Yuan et al. 2018; B. Wang et al. 2024). Thus, this method can also be applied to the study of the correlations within the gamma-ray band. For TeV radiation sources, luminosities in different observation bands are often correlated. By selecting one photometric band unaffected by EBL absorption and another that is affected, we can apply the maximum likelihood method to fit a copula function, thereby estimating the corresponding absorption optical depth. A key advantage of this approach is that it avoids assumptions about the intrinsic emission mechanisms or spectral shapes of TeV sources. Moreover, it can incorporate large datasets from multiple telescopes, enhancing

statistical robustness. Apart from the abovementioned reasons, another factor that may affect our calculations is the assumption about the cosmic emissivity. In this paper, we assume that the cosmic emissivity is a sum of normal templates with fixed peak positions, which may not be able to cover the true distribution of the cosmic emissivity. However, as we can see from the research results of Fermi-LAT Collaboration et al. (2018) and A. Desai et al. (2019), our assumption is reasonable. The results in Figure 3 also confirm the research findings of A. Domínguez et al. (2011) and A. Saldana-Lopez et al. (2021), that is, the SED template of the spiral-type galaxy is dominant.

Acknowledgments

The authors would like to thank the anonymous referee for the helpful comments, which improved the manuscript significantly. The authors gratefully acknowledge the financial support from the National Natural Science Foundation of China (grants 12063005, 12063006, 12233006, U2031111), the program for Innovative Research Team (in Science and Technology) in University of Yunnan Province (IRTSTYN), the program for Reserve Talents of Young and Middle-aged Academic and Technical Leaders in Yunnan Province (grants 202205AC160087, 202405AC350114), and the program for Hunan Outstanding Youth Science Foundation (2024JJ2040). The authors gratefully acknowledge the computing support provided by the JRT Science Data Center at Yuxi Normal University, and Q.L.H. gratefully acknowledges the kind and selfless help from Prof. Domínguez, A. (A. Domínguez et al. 2013).

ORCID iDs

Longhua Qin https://orcid.org/0000-0001-7905-4295
Jiancheng Wang https://orcid.org/0000-0003-0440-3109
Chuyuan Yang https://orcid.org/0000-0001-6903-5306
Quangui Gao https://orcid.org/0000-0001-9732-069X
Huaizhen Li https://orcid.org/0000-0001-8307-1442
Tingfeng Yi https://orcid.org/0000-0001-8920-0073
Zunli Yuan https://orcid.org/0000-0001-6861-0022
Chunxia Gu https://orcid.org/0009-0006-2334-3016

References

Albert, A., Alfaro, R., Alvarez, C., et al. 2022, ApJ, 933, 223
Abdalla, H., Razzaque, S., Böttcher, M., et al. 2024, MNRAS, 532, 198
Avila Rojas, D., Hernández-Cadena, S., González, M. M., et al. 2024, ApJ, 966, 114
Bernstein, R. A. 2007, ApJ, 666, 663
Bernstein, R. A., Freedman, W. L., & Madore, B. F. 2002, ApJ, 571, 107
Biteau, J. 2023, The Multi-Messenger Extragalactic Spectrum, v1.0., Zenodo, doi:10.5281/zenodo.7842239
Biteau, J., & Williams, D. A. 2015, ApJ, 812, 60
Buchner, J. 2021, JOSS, 6, 3001
Cao, Z., Aharonian, F., An, Q., et al. 2023, SciA, 9, eadj2778
Cao, Z., Chen, M.-J., Chen, S.-Z. H., et al. 2019, ChA&A, 43, 457
Desai, A., Ajello, M., Omodei, N., et al. 2017, ApJ, 850, 73
Desai, A., Helgason, K., Ajello, M., et al. 2019, ApJL, 874, L7
de Ugarte Postigo, A., Izzo, L., Pugliese, G., et al. 2022, GCN, 32648, 1
Domínguez, A., Finke, J. D., Prada, F., et al. 2013, ApJ, 770, 77
Domínguez, A., Primack, J. R., Rosario, D. J., et al. 2011, MNRAS, 410, 2556
Donath, A., Terrier, R., Remy, Q., et al. 2023, A&A, 678, A157
Dong, L. J., Zheng, Y. G., & Kang, S. J. 2023, ApJ, 952, 152
Dwek, E., & Krennrich, F. 2013, APh, 43, 112
Dwek, E., & Slavin, J. 1994, ApJ, 436, 696
Elbaz, D., Cesarsky, C. J., Fadda, D., et al. 1999, A&A, 351, L37
Fazio, G. G., Ashby, M. L. N., Barmby, P., et al. 2004, ApJS, 154, 39
Fermi-LAT Collaboration, Abdollahi, S., Ackermann, M., et al. 2018, Sci, 362, 1031
Finke, J. D., Ajello, M., Domínguez, A., et al. 2022, ApJ, 941, 33
Finke, J. D., & Razzaque, S. 2023, ApJL, 942, L21
Franceschini, A., Foffano, L., Prandini, E., et al. 2019, A&A, 629, A2
Franceschini, A., & Rodighiero, G. 2017, A&A, 603, A34
Gilmore, R. C., Somerville, R. S., Primack, J. R., et al. 2012, MNRAS, 422, 3189
Gréaux, L., Biteau, J., & Nievas Rosillo, M. 2024, ApJL, 975, L18
Hauser, M. G., Arendt, R. G., Kelsall, T., et al. 1998, ApJ, 508, 25
Hauser, M. G., & Dwek, E. 2001, ARA&A, 39, 249
H. E. S. S. Collaboration, Abdalla, H., Abramowski, A., et al. 2017, A&A, 606, A59
Inoue, Y., Inoue, S., Kobayashi, M. A. R., et al. 2013, ApJ, 768, 197
Koushan, S., Driver, S. P., Bellstedt, S., et al. 2021, MNRAS, 503, 2033
Lauer, T. R., Postman, M., Weaver, H. A., et al. 2021, ApJ, 906, 77
Lewis, A., & Bridle, S. 2002, PhRv, 66, 103511
LHAASO Collaboration, Cao, Z., Aharonian, F., et al. 2023, Sci, 380, 1390
Mackay, D. J. C. 2003, Information Theory, Inference and Learning Algorithms (UK: Cambridge Univ. Press), 640
Madau, P., & Dickinson, M. 2014, ARA&A, 52, 415
Madau, P., & Pozzetti, L. 2000, MNRAS, 312, L9
Mattila, K. 2006, MNRAS, 372, 1253
Matsumoto, T., Matsuura, S., Murakami, H., et al. 2005, ApJ, 626, 31
Meyer, M., Raue, M., Mazin, D., et al. 2012, A&A, 542, A59
Nelson, R. B. 2006, An Introduction to Copulas (Second Ed.; New York: Springer)
Papovich, C., Dole, H., Egami, E., et al. 2004, ApJS, 154, 70
Qin, L., Wang, J., Gao, Q., et al. 2023, MNRAS, 521, 6219
Saldana-Lopez, A., Domínguez, A., Pérez-González, P. G., et al. 2021, MNRAS, 507, 5144
Savage, R. S., & Oliver, S. 2005, arXiv:astro-ph/0511359
Stecker, F. W., & de Jager, O. C. 1993, ApJL, 415, L71
Wang, B., Liu, Y., Yu, H., et al. 2024, ApJ, 962, 103
Windhorst, R. A., Cohen, S. H., Jansen, R. A., et al. 2023, AJ, 165, 13
Wright, E. L. 2001, ApJ, 553, 538
Wright, E. L. 2004, NewAR, 48, 465
Yuan, Z., Wang, J., Worrall, D. M., et al. 2018, ApJS, 239, 33